Research Article

Lisa Davis, Monika Neda, Faranak Pahlevani, Jorge Reyes* and Jiajia Waters

A Numerical Study of a Stabilized Hyperbolic Equation Inspired by Models for Bio-Polymerization

https://doi.org/10.1515/cmam-2023-0222
Received October 10, 2023; revised February 23, 2024; accepted March 12, 2024

Abstract: This report investigates a stabilization method for first order hyperbolic differential equations applied to DNA transcription modeling. It is known that the usual unstabilized finite element method contains spurious oscillations for nonsmooth solutions. To stabilize the finite element method the authors consider adding to the first order hyperbolic differential system a stabilization term in space and time filtering. Numerical analysis of the stabilized finite element algorithms and computations describing a few biological settings are studied herein.

Keywords: Lighthill–Whitham–Richards Model, Greenshield's Velocity Model, Finite Element, DNA Transcription

MSC 2020: 65M12, 65M60, 92-08, 92-10

1 Introduction

Hyperbolic systems arise in a variety of applications including weather-forecasting, gas dynamics, modeling of shallow water, transport of contaminant in porous media, turbulent flows, granular flows and traffic flow [2, 5, 11, 21, 30, 35] . Modeling efforts for these applications have lead to the development of simulation methods capable of capturing complicated solution behavior. The first order hyperbolic system discussed in this paper is known to raise several challenges for the continuous Galerkin method. Optimal convergence on special cases of structured grids is known, but in general one can expect a loss of accuracy by one power of the mesh width [19, 45]. On general unstructured grids, besides the expected loss of one power in accuracy, for nonsmooth solutions the usual unstabilized FEM may also produce spurious oscillations [8]. Several stabilization methods have been introduced to correct this problem, such as the SUPG and SOLD method [7, 28], subgrid stabilization methods [23, 24], or filter based stabilization methods [10, 18, 21]. This work studies a stabilized finite element method that explores the use of both stabilization and filtering techniques in order to dampen spurious oscillations while preserving accuracy of solutions for such hyperbolic models.

The model problems considered here focus on the parallels between the study of traffic flow and the modeling of the bio-polymerization process. Protein synthesis is one example of bio-polymerization, a process characterized by forming polymers through the linking of monomers into a chain or network, typically accomplished through chemical reactions. Proteins, polypeptides and other fundamental building blocks of life are formed in this manner. Many types of mathematical models have been employed to describe this behavior, with some

***Corresponding author: Jorge Reyes,** Department of Mathematics, Virginia Tech, Blacksburg, VA 24061, USA, e-mail: reyesj@vt.edu. https://orcid.org/0000-0002-5096-2297
Lisa Davis, Department of Mathematical Sciences, Montana State University, Bozeman, MT 59717, USA, e-mail: lisa.davis@montana.edu
Monika Neda, Department of Mathematical Sciences, University of Nevada Las Vegas, Las Vegas, NV 89154, USA, e-mail: monika.neda@unlv.edu
Faranak Pahlevani, Division of Science & Engineering, Penn State University Abington, Abington, PA 19001, USA, e-mail: fxp10@psu.edu
Jiajia Waters, Los Alamos National Laboratory, Los Alamos, USA, e-mail: jwaters@lanl.gov

models dating back as far as the 1960s and ranging through present day, see [6, 9, 11, 27, 31, 36, 37, 39, 41, 43, 47]. There is a natural correspondence between some bio-polymerization models and those applied to traffic flow as the two phenomena are quite similar. Bio-polymerization is characterized by the motion of a molecular motor (RNA polymerase or RNAp) copying a segment of a gene. To continue the analogy, consider the case when there are many RNAPs transcribing the gene simultaneously. This can be compared to the situation where many cars are present on a stretch of roadway. In both cases, the total flux depends on the density and velocity. The Greenshield's model makes the additional assumption that velocity depends on density with higher densities resulting in slower speeds and vice versa. For further biological context, see Section 1.2.

Recently a first order traffic flow model has been used to explore the transcription and translation phenomena [11–13]. The simplest of these first order models is the Lighthill–Whitham–Richards Model, commonly known as the LWR model, which was proposed by researchers in the 1950s in order to analyze and quantify traffic flow behavior. Here we use the LWR model as a prototype for the application of bio-polymerization since it provides a robust set of motivating test problems for evaluating the effectiveness of the stabilization and time filter techniques.

1.1 Continuum Models

The LWR model was introduced in the mid-1950s as a one-dimensional macroscopic model to study traffic flow phenomena. Within this fluid-dynamic model, the traffic was considered to be an inviscid but compressible fluid, and the traffic flow variables: density ρ, velocity v and flow f, were defined as continuous quantities in time and space. According to this model, the traffic flow f is defined to be a function of density and velocity defined according to the relation $f = \rho v$. The density evolves according to the conservation law

$$\frac{\partial}{\partial t}\rho(t,x) + \frac{\partial}{\partial x}f(t,x) = 0, \tag{1.1}$$

where ρ represents the average traffic density of the vehicles in time and space.

When one assumes that the traffic velocity is a constant, $v = \bar{v}$, then the linear form of the LWR model to be used in this work is given with boundary and initial conditions specified as

$$\begin{cases} \frac{\partial}{\partial t}\rho + \bar{v}\frac{\partial}{\partial x}\rho = 0, \quad 0 < x \le 1,\ t > 0, \\ \qquad \rho(x,0) = \rho_0, \\ \qquad \rho(0,t) = \rho_I. \end{cases} \tag{1.2}$$

This equation is well known as the linear advection equation with advection speed $\bar{v}$. Analytical solutions are known, and it is amenable to a full analysis for approximation schemes.

A more realistic relationship between the flow velocity and traffic density was developed by Greenshield in [20]. In that case, the Greenshield's velocity model connects the traffic density ρ to the traffic velocity v with the following linear relationship:

$$v(\rho) = v_f\left(1 - \frac{\rho}{\rho_m}\right), \tag{1.3}$$

where v_f is the free flow speed and ρ_m is the maximum jam density. The free flow speed v_f represents the speed of the traffic when the density ρ is zero. The maximum density ρ_m is the traffic density at which the speed of traffic v is equal to zero. Due to the relation shown in equation (1.3), the graph between the flux f and the density ρ assumes a concave shape, since $\frac{\partial^2 f}{\partial \rho^2} < 0$. This relationship between density, flow, and velocity is shown in Figure 1.

The LWR with the Greenshield's model is

$$\frac{\partial \rho}{\partial t} + \left(v_f - \frac{2v_f}{\rho_m}\rho\right)\frac{\partial \rho}{\partial x} = 0. \tag{1.4}$$

It is known that when we solve the hyperbolic traffic flow PDE given by equation (1.4), oscillations exist around the shock solutions. Herein we apply a stabilization of FEM introduced in [18] for the advection equation

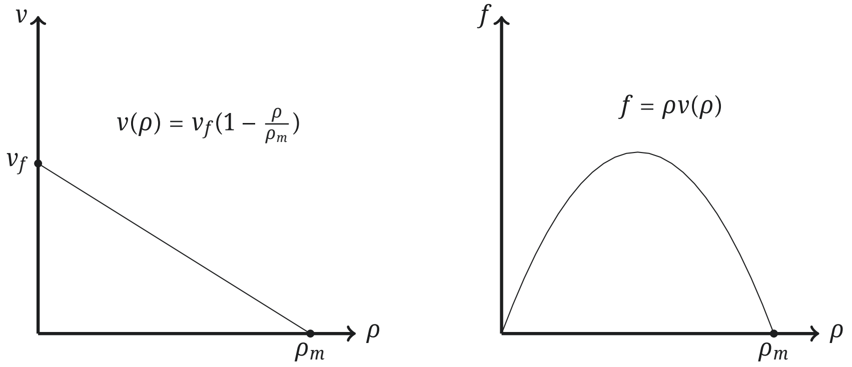

(a) Greenshield's model for velocity.

(b) Flux based on Greenshield's model.

Figure 1: Experimental relationship between density, flow and velocity based on LWR and Greenshield's model.

based on Vreman filtering [46]. Additionally, we use a simple time filter (2.6) first introduced in [25] for the backward Euler method. This time filter does not add computational complexity and is shown to be second order accurate in time when added to backward Euler schemes for the Navier–Stokes equations [15, 25]. This concept of utilizing linear time filters was generalized for other common time stepping schemes in [14].

In [4] the time filter is shown to be effective at improving accuracy when combined with an explicit first order upwind finite difference method with minimal expense in numerical implementation for the linear case in (1.2). There the filtered scheme introduces a small amount of dissipation into the behavior of a nonsmooth solution, thereby increasing accuracy while preventing spurious oscillations. This paper follows a similar approach to [4] where analysis techniques originally used for the Vreman stabilization algorithm are applied in order to analyze the time filtered, Vreman stabilized Galerkin scheme for both linear and nonlinear cases.

1.2 Motivating Biological Application

Transcription and translation are two key stages of protein synthesis and are crucial components in the transfer of genetic information from DNA to protein during cell growth. Transcription involves the transfer of genetic information from DNA to several types of RNA including messenger mRNA (mRNA), transfer RNA (tRNA), ribosomal RNA (rRNA) and others. This process involves separation of the two DNA strands and synthesis of an RNA molecule by the enzyme RNA polymerase(RNAP), using one of the DNA strands as a template. Transcription begins when the RNAP binds to a promoter sequence of a gene (*initiation*) and then proceeds through the *elongation* process. During elongation, the RNAP motors along the coding region of the gene, reading the DNA strand, and generating a single-stranded RNA copy. Transcription ends at the gene's *termination* region, where the RNAP releases the nascent copy of the RNA and unbinds from the DNA strand. If the resulting RNA strand is mRNA, it is then translated by a ribosome to a chain of amino acids that fold to produce a protein. If the resulting RNA is rRNA or tRNA, it is not translated, but it provides a scaffold to facilitate binding of other proteins to form RNA-protein complexes such as ribosomes, another important genetic building block for cellular growth.

In the context of the continuum model given in (1.2), the assumption that the RNAP velocity $v = \bar{v}$ is constant characterizes the situation where the elongation velocity of all RNAPs transcribing the gene is constant along the entire spatial extent of the strand and for all time. For a full description of the biological parameters associated with the use of this model to describe transcription for a prototypical example of a gene in the bacteria E. coli, the reader is referred to [13]. That work includes a description of the non-dimensionalization process leading to the dimensionless equation in (1.2), and the relationship of the parameters ρ_0 and ρ_I to the initiation rate, maximal elongation velocity, and maximum density for RNAPs on the gene can be found in [13, Appendix]. A numerical analysis of the time filtered upwind scheme for approximating the solution of (1.2) can be found in [4]. The numerical results for the linear case presented in this work are also limited to the case where $\bar{v} = 1$, although the analysis is performed for the more general case of an arbitrary advection speed.

The *translation* process is similar to that of transcription. Ribosomes translate mRNA strands in order to generate ribosomal proteins which form the scaffolding for building new ribosomes, hence promoting cell growth. During *translation* ribosomes act as the molecular motor as they read the genetic information on an mRNA strand, and the initiation, elongation, and termination phases occur in the same fashion as described above. Although these processes require availability of various amino acids, as well as assembly of several initiator and termination complexes, we focus on a simple model describing the more mechanical processes of transcription (and translation) for the sake of simplicity in this paper.

While the density of RNAPs on most genes is believed to be low, there are examples of genes, such as the rrn operon, in the bacteria E. coli where the density of RNAPs is observed to be very high. That is, there are many RNAPs transcribing the gene simultaneously. This can be compared to the situation where many cars are present on a stretch of roadway. For such genes, transcriptional elongation of RNAPs is not uniform, and this can result in spatial regions of the gene where the density of RNAPs is quite high and other regions of the gene where the density is low [16].

Simulation methods that can accurately resolve the model behavior for a nonuniform density profile are essential to building a high fidelity model for bio-polymerization processes. In this work, we consider examples of model problems where the density along the strand has a significant variation initially and explore the simulation results for the numerical filtering techniques introduced.

This article is organized as follows. In Section 2 we cover preliminaries about the finite element method and introduce the algorithms. Section 3 gives the stability results of the algorithms of interest. Then we present four model problems and their numerical simulation results that support the theoretical results in Section 4. Two simulation tests for the linear Algorithm 1 were performed. The convergence rate calculations are explored in Section 4.2, and results for a traveling discontinuous wavefront are given in Section 4.3. For the nonlinear Algorithm 2, we performed simulation studies using the stationary shock problem outlined in Section 4.4 and the discontinuous initial density problem in Section 4.5. We conclude our work in the last Section 5.

2 Notation, Preliminaries and Algorithms

2.1 Notation and Preliminaries

Let $\Omega \subset \mathbb{R}$ denote the domain, while the $L^2(\Omega)$ norm and the inner product are denoted by $\|\cdot\|$ and $(\cdot,\cdot)$, respectively. Similar to what is used in [10, 18] the function spaces used is the closure of C^∞, periodic functions on Ω in the H^1 norm denoted as $X := H^1_\#(\Omega)$. Let $X_h \subset X$ be the finite element subspace.

The continuous mean $\overline{u} \in X$ of $u \in X$ is the solution of the PDE (see [22])

$$-\delta^2 \Delta \overline{u} + \overline{u} = u,$$

and the discrete mean $\overline{u}^h \in X_h$ of $u \in X$ (see [38]) is defined as the unique solution of

$$\delta^2 (\nabla \overline{u}^h, \nabla v_h) + (\overline{u}^h, v_h) = (u, v_h) \quad \text{for all } v_h \in X_h,$$

where the mean quantities are associated with the filtering length scale δ.

The mathematical stability and accuracy properties of continuous and discrete averaging and deconvolution have been studied in [3, 17, 32–34, 38]. The operators denoted as $\overline{\cdot}$ and $\overline{\cdot}^h$ represent filtering and they lend the physical meaning to the parameter δ as the filter width. In the finite element setting, we have $\delta = O(h)$, where h is the mesh size of our finite element discretization. We give a few properties and a lemma used in our analysis below. Lemma 1 is a convenient algebraic identity from [15] which will be used in a similar manner for the stability analysis.

Lemma 1 ([15]). *The following identity holds:*

$$\Big(\frac{3}{2}a - 2b + \frac{1}{2}c\Big)\Big(\frac{3}{2}a - b + \frac{1}{2}c\Big) = \frac{1}{4}(a^2 + (2a-b)^2 + (a-b)^2) - \frac{1}{4}(b^2 + (2b-c)^2 + (b-c)^2) + \frac{3}{4}(a - 2b + c)^2.$$

Next we introduce two variational formulations for LWR model with constant velocity and Greenshield's (linear) model of velocity. A stabilization term is added to both formulations.

Thus, a stabilized finite element variational formulation of (1.2) can be stated as: Find discrete finite element density $\rho_h \in X_h$ satisfying

$$\begin{cases} \Big(\frac{\partial}{\partial t}\rho_h, v_h\Big) + \overline{v}\Big(\frac{\partial}{\partial x}\rho_h, v_h\Big) + \chi\delta^2\Big(\frac{\partial}{\partial x}\rho_h^*, \frac{\partial}{\partial x}v_h^*\Big) = 0 & \text{for all } v_h \in X_h, \\ \rho(x,0) = \rho_0(x) & \text{for all } x \in \Omega, \end{cases} \tag{2.1}$$

where the new stabilization term $\chi\delta^2(\frac{\partial}{\partial x}\rho^*, \frac{\partial}{\partial x}v_h^*)$, initially introduced by Vreman [46] is added. Here

$$\rho^* = \rho - \overline{\rho}^h$$

the goal of this term is to improve accuracy and damp unwanted spurious oscillations while being cheap computationally to implement. This also introduces the dimensionless χ as a stabilization parameter which can be manually tuned to increase or decrease the affects of the added stabilization term.

From [29] we also define trilinear term $b(\cdot,\cdot,\cdot) : X \times X \times X \mapsto \mathbb{R}$ as

$$b(u,v,w) = \frac{1}{3}\int_\Omega ((uv)' + uv')w\,dx. \tag{2.2}$$

In [29, 42] it is proven that b is skew-symmetric, i.e.,

$$b(u,v,w) + b(u,w,v) = 0. \tag{2.3}$$

Furthermore, a stabilized finite element variational formulation of (1.4) can be stated as: Find $\rho_h \in X_h$ satisfying

$$\Big(\frac{\partial}{\partial t}\rho_h, v_h\Big) + v_f\Big(\frac{\partial}{\partial x}\rho_h, v_h\Big) - \frac{2v_f}{\rho_m}b(\rho_h,\rho_h,v_h) + \chi\delta^2\Big(\frac{\partial}{\partial x}\rho_h^*, \frac{\partial}{\partial x}v_h^*\Big) = 0 \quad \text{for all } v \in X_h. \tag{2.4}$$

2.2 Time Filtered Vreman Stabilization Algorithm

For all numerical simulations presented in Section 4 we employ the Backward Euler temporal discretization. Additionally, we implement the time filter studied in [13, 15, 25] as a post processing step to the Backward Euler scheme for approximating the density ρ^n from the intermediate density approximation from Step 1, i.e., $\hat{\rho}^n$. This increases our algorithms to second order convergence in time. The discretized finite element algorithms for time interval $(0, T]$ are stated below:

Algorithm 1 (Fully Discrete Method for linear case). For $n = 2, 3, \dots, N_T$, find $\rho_h^n \in X_h$ such that

- *Step 1: Backward Euler*

$$\frac{1}{\Delta t}(\hat{\rho}_h^n - \rho_h^{n-1}, v_h) + \bar{v}\Big(\frac{\partial}{\partial x}\hat{\rho}_h^n, v_h\Big) + \chi\delta^2\Big(\frac{\partial}{\partial x}\hat{\rho}_h^{n^*}, \frac{\partial}{\partial x}v_h^*\Big) = 0 \quad \text{for all } v_h \in X_h, \tag{2.5}$$

- *Step 2: Time Filter*

$$\rho_h^n = \hat{\rho}_h^n - \frac{\gamma}{2}(\hat{\rho}_h^n - 2\rho_h^{n-1} + \rho_h^{n-2}). \tag{2.6}$$

Algorithm 2 (Fully Discrete Method for Greenshield's model). For $n = 2, 3, \dots, N_T$ find $\rho_h^n \in X_h$ such that

- *Step 1: Backward Euler*

$$\frac{1}{\Delta t}(\hat{\rho}_h^n - \rho_h^{n-1}, v_h) + v_f\Big(\frac{\partial}{\partial x}\hat{\rho}_h^n, v_h\Big) - \frac{2v_f}{\rho_m}b(\hat{\rho}_h^n, \hat{\rho}_h^n, v_h) + \chi\delta^2\Big(\frac{\partial}{\partial x}\hat{\rho}_h^{n^*}, \frac{\partial}{\partial x}v_h^*\Big) = 0 \quad \text{for all } v_h \in X_h, \tag{2.7}$$

- *Step 2: Time Filter*

$$\rho_h^n = \hat{\rho}_h^n - \frac{\gamma}{2}(\hat{\rho}_h^n - 2\rho_h^{n-1} + \rho_h^{n-2}).$$

By choosing $\gamma = \frac{2}{3}$ in the time filter equation in the above algorithm and then solving it for the intermediate density $\hat{\rho}_h^n$ obtained from the Backward Euler in Step 1, we get

$$\hat{\rho}_h^n = \frac{3}{2}\rho_h^n - \rho_h^{n-1} + \frac{1}{2}\rho_h^{n-2}. \tag{2.8}$$

Replacing $\hat{\rho}_h^n$ in Step 1 by (2.8), one can reduce the two step process in Algorithm 2 to a single equation process. For simplicity in notation and later in the stability analysis, we first introduce the interpolation and difference operators given below:

$$I[\rho^n] = \frac{3}{2}\rho^n - \rho^{n-1} + \frac{1}{2}\rho^{n-2}, \tag{2.9}$$

$$D[\rho^n] = \frac{3}{2}\rho^n - 2\rho^{n-1} + \frac{1}{2}\rho^{n-2}. \tag{2.10}$$

Incorporating (2.9) and (2.10) into Algorithm 2 and using (2.8), we obtain the following equivalent scheme:

$$\frac{1}{\Delta t}(D[\rho_h^n], v_h) + v_f\Big(\frac{\partial}{\partial x}I[\rho_h^n], v_h\Big) - \frac{2v_f}{\rho_m}b(I[\rho_h^n], I[\rho_h^n], v_h) + \chi\delta^2\Big(\frac{\partial}{\partial x}I[\rho_h^n]^*, \frac{\partial}{\partial x}v_h^*\Big) = 0. \tag{2.11}$$

The initial condition ρ_h^0 is the L_2 projection of ρ_0 and ρ_h^1 is obtained using Backward Euler.

3 Stability Analysis

Lemma 2. *Solutions to the semi-discrete scheme* (2.4) *are stable and satisfy*

$$\|\rho_h\|^2 + \chi\delta^2 \int_0^t \Big\|\frac{\partial}{\partial x}\rho_h^*\Big\|^2 \, d\tau \le \|\rho_0\|^2. \tag{3.1}$$

Proof. Choosing $v_h = \rho_h$ in (2.4) yields

$$\frac{1}{2}\frac{\partial}{\partial t}\|\rho_h\|^2 - \frac{2v_f}{\rho_m}b(\rho_h, \rho_h, \rho_h) + \chi\delta^2\Big\|\frac{\partial}{\partial x}\rho_h^*\Big\|^2 = -v_f\Big(\frac{\partial}{\partial x}\rho_h, \rho_h\Big). \tag{3.2}$$

Since b is skew-symmetric, the nonlinear term vanishes. The right-hand side term also vanishes due to the following argument using the periodic boundary conditions and fundamental theorem of Calculus

$$-v_f\Big(\frac{\partial}{\partial x}\rho_h, \rho_h\Big) = -v_f \int_\Omega \frac{\partial \rho_h}{\partial x}\rho_h \, dx = -v_f \int_\Omega \frac{1}{2}\frac{\partial}{\partial x}\,|\rho_h|^2 \, dx = 0. \tag{3.3}$$

Then multiplying by 2 and integrating over time, we obtain

$$\|\rho_h\|^2 + 2\chi\delta^2 \int_0^t \Big\|\frac{\partial}{\partial x}\rho_h^*\Big\|^2 \, d\tau \le \|\rho_h^0\|^2, \tag{3.4}$$

where ρ_h^0 is taken to be the L^2 projection of ρ_0 which yield the result. □

Lemma 3. *The solutions to the fully discrete scheme* (2.11) *are unconditionally stable and satisfy*

$$\|\rho_h^N\|^2 + 4\sum_{n=2}^N \mathcal{Z}^n + 2\chi\delta^2\Delta t \sum_{n=2}^N \Big\|\frac{\partial}{\partial x}I[\rho_h^n]^*\Big\|^2 \le C(\rho_0, \rho_1), \tag{3.5}$$

where

$$\mathcal{E}^n = \frac{1}{4}(\|\rho_h^n\|^2 + \|2\rho_h^n - \rho_h^{n-1}\|^2 + \|\rho_h^n - \rho_h^{n-1}\|^2), \tag{3.6}$$

$$\mathcal{Z}^n = \frac{3}{4}\|\rho_h^n - \rho_h^{n-1} - \rho_h^{n-2}\|^2. \tag{3.7}$$

Proof. Choosing $v_h = I[\rho_h^n]$ in (2.11) yields

$$\frac{1}{\Delta t}(D[\rho_h^n], I[\rho_h^n]) - \frac{2v_f}{\rho_m} b(I[\rho_h^n], I[\rho_h^n], I[\rho_h^n]) + \chi\delta^2 \left\| \frac{\partial}{\partial x} I[\rho_h^n]^* \right\|^2 = -v_f\left(\frac{\partial}{\partial x} I[\rho_h^n], I[\rho_h^n]\right). \tag{3.8}$$

By Lemma 1, the first term results in

$$(D[\rho_h^n], I[\rho_h^n]) = \mathcal{E}^n - \mathcal{E}^{n-1} + \mathcal{Z}^n. \tag{3.9}$$

The nonlinear term vanishes. Similarly to what is done in Lemma 2 the term on the right-hand side vanishes as well

$$v_f\left(\frac{\partial}{\partial x} I[\rho_h^n], I[\rho_h^n]\right) = v_f \int\limits_\Omega I[\rho_h^n] \frac{\partial}{\partial x} I[\rho_h^n]\, dx = \frac{1}{2} \int\limits_\Omega \frac{\partial}{\partial x} |I[\rho_h^n]|^2\, dx = 0. \tag{3.10}$$

After multiplying by Δt and simplifying

$$\mathcal{E}^n - \mathcal{E}^{n-1} + \mathcal{Z}^n + \Delta t \frac{\chi\delta^2}{2} \left\| \frac{\partial}{\partial x} I[\rho_h^n]^* \right\|^2 \leq 0.$$

Summing from $n = 2, \dots, N$ gives

$$\mathcal{E}^N + \sum_{n=2}^{N} \mathcal{Z}^n + \frac{\chi\delta^2}{2} \Delta t \sum_{n=2}^{N} \left\| \frac{\partial}{\partial x} I[\rho_h^n]^* \right\|^2 \leq \mathcal{E}^1.$$

Based on definition of $\mathcal{E}^N$ from (3.6) and bounds of the initial conditions we achieve the desired result. □

Remark 1. Both the semi-discrete scheme (2.1) and fully discrete Algorithm (1) are also stable and satisfy (3.1) and (3.5) respectively. The proof follows the same steps as in Lemma 2 and Lemma 3.

Remark 2. For the case of linear advection considered in (1.2), it is well-known that explicit finite difference and finite volume schemes must choose a discretization that satisfies a CFL condition to ensure stability [35, 40, 44]. The presented time stepping algorithm with the corresponding time filtered technique however, as an implicit linear multistep time stepping method, is unconditionally stable as shown in Lemma 3.

4 Computational Experiments

4.1 Algorithm Implementation

For the Fully Discrete Method for linear case, (2.5) can be written as follows: For $n = 2, 3, \dots, N_T$ find $\rho_h^n \in X_h$ such that

$$\frac{1}{\Delta t}(\hat{\rho}_h^n - \rho_h^{n-1}, v_h) + \bar{v}\left(\frac{\partial}{\partial x}\hat{\rho}_h^n, v_h\right) + \chi\delta^2\left(\frac{\partial}{\partial x}\hat{\rho}_h^{n^{**}}, \frac{\partial}{\partial x} v_h\right) = 0 \quad \text{for all } v_h \in X_h, \tag{4.1}$$

where the $*$ operator is the same as in equation (2.1). Herein $\hat{\rho}_h^{n^{**}}$ cannot be treated explicitly. We used a fixed point iteration on the implicit terms. Pseudo-code for this case, $\hat{\rho}_h^{n^{**}} = \hat{\rho}_h^n - 2\bar{\hat{\rho}}_h^n + \bar{\bar{\hat{\rho}}}_h^n$, when $\hat{\rho}_h^n$ is computed is given as:

```
$\hat{\rho}_h^n \leftarrow \hat{\rho}_h^{n-1}$
for k=0, MaxIteration , +1 do
    $\hat{\rho}_{h,\text{old}}^n = \hat{\rho}_h^n$
    $w = \bar{\hat{\rho}}_h^n$
    % Solve for
    $\frac{1}{\Delta t}(\hat{\rho}_h^n - \hat{\rho}_h^{n-1}, v_h) + \bar{v}(\frac{\partial}{\partial x}\hat{\rho}_h^n, v_h) + \chi\delta^2(\frac{\partial}{\partial x}(\hat{\rho}_h^n - 2w + \bar{w}), \frac{\partial}{\partial x} v_h) = 0$ for all $v_h \in X_h$
    if $\|\hat{\rho}_{h,\text{old}}^n - \hat{\rho}_{h,\text{old}}^n\| <$ tolerance break then
    end if
end for
```

The tolerance used in subsequent simulations was set to 10^{-8}. The true solution was used to compute the initial condition for all simulations. All of the experiments are implemented in FreeFem++ version 4.4.3 [26] and data visualizations are done using Paraview version 5.7.0 [1] along with Python's matplotlib library.

4.2 Convergence Rate Calculations

In this subsection, we utilize the following test problem with the choice of $\bar{v} = 1$ to calculate the model's rate of convergence in terms of Δt and mesh size $h = \Delta x$:

$$\begin{cases} \rho_t + \rho_x = 0, & 0 < x \le 1,\ 0 < t \le 1, \\ \rho(x,0) = \sin 2\pi x, & 0 \le x \le 1, \\ \rho(0,t) = -\sin 2\pi t, & t > 0. \end{cases} \tag{4.2}$$

The true solution of (4.2) is known to be $\rho(x,t) = \sin(2\pi(x-t))$. The approximations are using $P2$ finite elements and all simulations are performed up to the final time $T = 1$. The choice of parameters $\chi = 2500$ and $\delta = 0.02h^{0.5}$ is based on the test of error estimate in [18]. Table 1 demonstrates the convergence rate for Δt with a set mesh width as $h = 0.001$ and a refined time step by a factor of half. Based on the numbers listed in Table 1, backward Euler, $\gamma = 0$, delivers the expected rate of convergence equal to 1 while with added time filter using the time filter parameter, $\gamma = \frac{2}{3}$, the rate of convergence increases in value to 2.

The expected rate of convergence in terms of spatial refinement for the approximated density can be drawn from the theoretical convergence results in [18] using Corollary 3.2 therein.

For quadratic finite element polynomial approximation $k = 2$ and the choice of $\delta = 0.02h^{0.5}$, the spatial rate of convergence for the approximated density in (4.2) is expected to be 1.5. Tables 2 and 3 demonstrate the spatial rate for $\Delta t = 2^{-16} \approx 0.00002$ and $\Delta t = 2^{-12} \approx 0.0002$ set values respectively. We start with $h = \frac{1}{8}$ and

	$\|\rho - \rho_h\|_{\ell^\infty(0,T;L^2)}$ Error			
Δt	$\gamma = 0$	Rate	$\gamma = \frac{2}{3}$	Rate
$\frac{1}{16}$	0.0106812	–	0.00921303	–
$\frac{1}{32}$	0.0063397	0.75	0.00270058	1.77
$\frac{1}{64}$	0.00349665	0.86	0.000699355	1.95
$\frac{1}{128}$	0.00184422	0.92	0.000176171	1.99
$\frac{1}{256}$	0.000948405	0.96	4.41688×10^{-5}	2.00
$\frac{1}{512}$	0.000481157	0.99	1.11346×10^{-5}	1.99

Table 1: Numerical errors and rates in time for Algorithm 1 for $h = 0.001$, $\chi = 2500$ and $\delta = 0.02h^{0.5}$.

	$\|\rho - \rho_h\|_{\ell^\infty(0,T;L^2)}$ Error			
h	$\gamma = 0$	Rate	$\gamma = \frac{2}{3}$	Rate
$\frac{1}{8}$	0.00354754	–	0.00352879	–
$\frac{1}{16}$	0.000818518	2.12	0.000812389	2.12
$\frac{1}{32}$	0.000302091	1.44	0.000298696	1.44
$\frac{1}{64}$	0.000107899	1.49	0.000106262	1.49
$\frac{1}{128}$	3.7559×10^{-5}	1.52	3.59366×10^{-5}	1.56

Table 2: Numerical errors and rates in space for Algorithm 1 for $\Delta t \approx 0.00002$, $\chi = 2500$ and $\delta = 0.02h^{0.5}$.

	$\|\rho - \rho_h\|_{\ell^\infty(0,T;L^2)}$ Error			
h	$\gamma = 0$	Rate	$\gamma = \frac{2}{3}$	Rate
$\frac{1}{8}$	0.00387709	–	0.00352889	–
$\frac{1}{16}$	0.00101808	1.93	0.000812653	2.12
$\frac{1}{32}$	0.000480005	1.08	0.000298809	1.44
$\frac{1}{64}$	0.000274581	0.81	0.000106268	1.49
$\frac{1}{128}$	0.000178078	0.62	3.59569×10^{-5}	1.56

Table 3: Numerical errors and rates in space for Algorithm 1 for $\Delta t \approx 0.0002$, $\chi = 2500$ and $\delta = 0.02h^{0.5}$.

refine, halving each time. Table 2 shows that for a sufficiently small time step, i.e., $\Delta t = 2^{-16}$, both methods achieve the same theoretically predicted rate of 1.5. For a larger time step, e.g., $\Delta t = 2^{-12}$, Table 3 shows that the traditional Backward Euler, $\gamma = 0$, has suboptimal performance while the time filtered scheme maintains the expected theoretical convergence rate of 1.5. A possible explanation is that the time filter method is second order in time and thus gives smaller errors in time without polluting the spatial error.

4.3 Traveling Discontinuous Waveform Problem

Here we study the linear advection test problem in (1.2) with $\bar{v} = 1$, $\rho_0 = 0$ and $\rho_I = 0.47$. In the context of the motivating biological application, equation (4.3) models the case where the RNAP elongation velocity is constant under all conditions, the DNA strand is initially empty of any RNAPs and the initiation of RNAPs occurs at a rate which corresponds to a density of RNAPs described by $\rho_I = 0.47$. The solution to this model problem is discontinuous for $t > 0$, and the discontinuity propagates across the domain with speed 1. The discontinuity advects, or travels, along the characteristics $x - t = c$ in the domain, where $c > 0$ is any constant.

$$\begin{cases} \rho_t + \rho_x = 0, & 0 < x \le 1,\ 0 < t \le 1, \\ \rho(x,0) = 0, & 0 \le x \le 1, \\ \rho(0,t) = 0.47, & t > 0. \end{cases} \tag{4.3}$$

This test problem is considered in [13] where the time filter is applied to the classical explicit (finite difference) upwind scheme. In that case, the time filter is shown to improve the accuracy of the approximation scheme; however, the convergence rate of the filtered scheme remains the same as that of the unfiltered upwind scheme. Here it is shown that the time filter improves the convergence rate of the unfiltered backward Euler approach.

We use $P2$ elements, and the time filter is implemented for all simulation results shown in this work. In Figure 2 we use $h = 0.02$, $\chi = \delta = 0$, while we vary the size of time steps ($\Delta t = 2^{-6} \approx 0.016$, $\Delta t = 2^{-8} \approx 0.004$, and $\Delta t = 2^{-10} \approx 0.001$). We observe that as the time step size decreases, the more accurately we capture the solution's discontinuous profile. For that reason, we use $\Delta t = 2^{-10}$ for all subsequent simulations in this subsection. In addition, we note that all simulations have spurious oscillations that were removed with the addition of the Vreman stabilization term; see Figures 3–6.

Figures 3 and 4 illustrate the effects that δ and χ have on numerical solutions. Mathematically since they both appear as scalars on the same term in Algorithm 1, not the semi-discrete or the fully-discrete algorithm, it is expected that they share the same affect. This can be seen in both figures where the amount of "damping" increases with increases in both δ and χ. This damping introduces dissipation into the approximation scheme, which causes the "smoothing" out of the shock profile. Hence, it can be inferred that selecting small values for both δ and χ is desirable. However, Figure 4 shows that choosing too small a value ($\chi = 0.01$) results in a failure to remove the spurious oscillations present in the unstabilized model. For that reason, we choose $\delta = h$ and $\chi = 1$ for the last Figures 5 and 6.

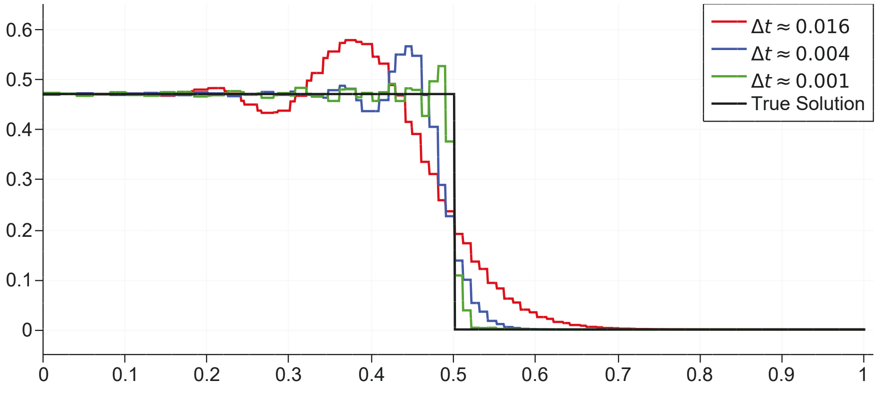

Figure 2: Comparisons of numerical solutions at t=0.5 with varying time-steps, $h = 0.02$ and $\chi = \delta = 0$.

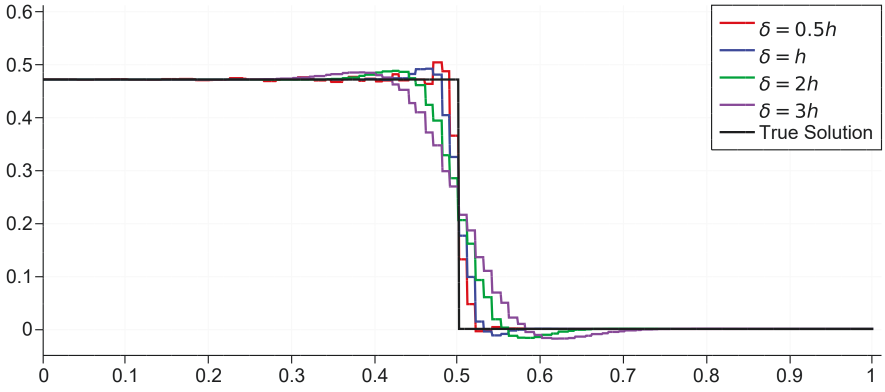

Figure 3: Comparisons of numerical solutions at t=0.5 with time step $\Delta t \approx 0.001$, $\chi = 1$, $h = 0.02$, and various values for δ.

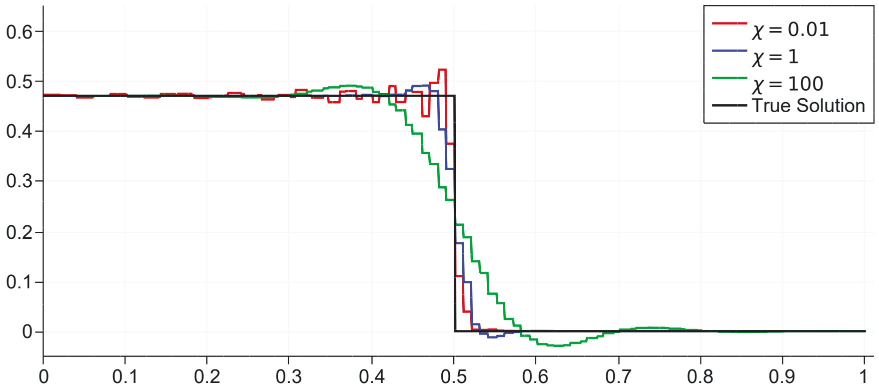

Figure 4: Comparisons of numerical solutions at t=0.5 with time step $\Delta t \approx 0.001$, $\delta = h$, $h = 0.02$, and various values for χ.

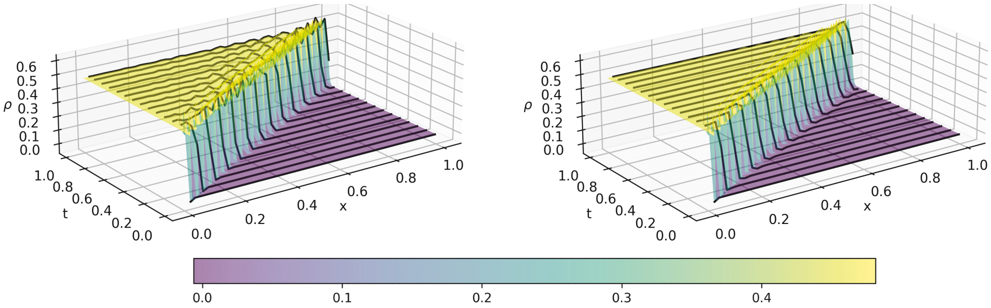

Figure 5: Numerical results of Algorithm 1 ($\chi = 0$, left and $\chi = 1$, right) with $\Delta t \approx 0.001$, $h = 0.02$, $\delta = h$.

These figures illustrates the effect of adding the Vreman stabilization term over time. Here we use $h = 0.02$, $\Delta t = 2^{-10} \approx 0.001$, and the total number of time steps is 1024. Figure 6 shows a cross section of Figure 5 at three specific time steps. As can be seen the addition of the Vreman filter based stabilization significantly removes spurious oscillations present in the unstabilized model overtime.

4.4 Stationary Shock

We now investigate problem (4.4) where the parameters of the problem are chosen carefully to ensure that the solution is discontinuous at $x = 0.5$ for all time t. We note that such choices are somewhat of an idealized biological situation where the environmental factors would have to be specified precisely; however, this example

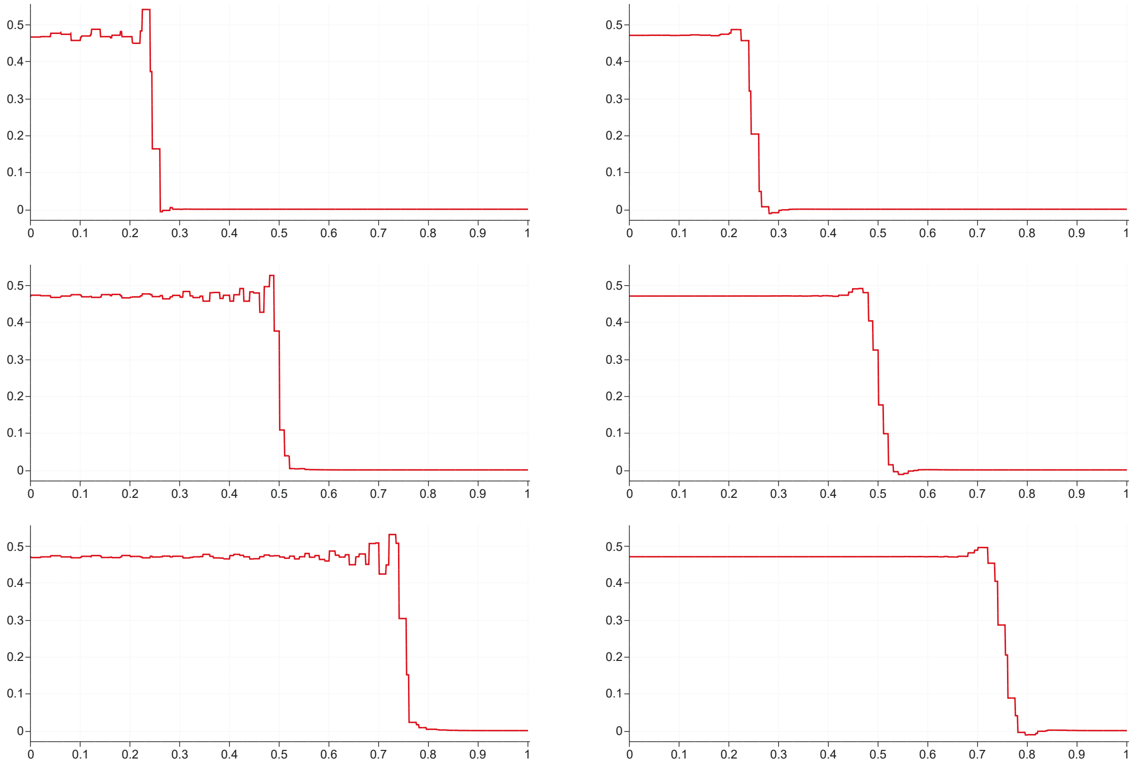

Figure 6: Numerical results of Algorithm 1 ($\chi = 0$, left and $\chi = 1$, right) at times $t = 0.25, 0.5, 0.75$ (top to bottom) with $\Delta t \approx 0.001$, $h = 0.02$, $\delta = h$.

provides an interesting example of the need for precise tuning of the stabilization parameters in order to ensure stability for the case of a stationary shock:

$$\begin{cases} \rho_t + v_f \rho_x - \dfrac{2v_f}{\rho_m} \rho \rho_x = 0, \quad 0 \le x \le 1,\ 0 < t \le 4, \\ \rho(0,t) = 0, \quad t > 0, \\ \rho(x,0) = \begin{cases} \rho_l, & 0 \le x < 0.5, \\ \rho_r, & 0.5 < x \le 1. \end{cases} \end{cases} \tag{4.4}$$

We assign the following parameters the values of $\rho_m = 0.47$, $v_f = 1$, $\rho_l = 0$ and $\rho_r = 0.47$. A shock stays stationary if $\rho_l = \rho(0.5^-, 0)$ and $\rho_r = \rho(0.5^+, 0)$ are chosen such that the shock velocity remains zero.

Based on the parameters ρ_l and ρ_r, the initial density profile we get for this problem is shown in Figure 7. For the chosen ρ_l and ρ_r, the shock speed can be computed as

$$\lambda = \frac{f(\rho_r) - f(\rho_l)}{\rho_r - \rho_l} = \frac{\rho_l v_f (1 - \frac{\rho_l}{\rho_m}) - \rho_r v_f (1 - \frac{\rho_r}{\rho_m})}{\rho_l - \rho_r},$$

$$\lambda = \frac{(0.47)(1)(1 - \frac{0.47}{0.47}) - (0)(1)(1 - \frac{0}{0.47})}{0.47 - 0} = 0,$$

where $f(\rho) = \rho v = v_f \rho (1 - \frac{\rho}{\rho_m})$ for this example. Thus, we have a shock speed of $\lambda = 0$ resulting in the shock remaining stationary for all time $t > 0$.

For the computational results, we use $P2$ elements time filtering for all simulations and a final time $T = 3$. In Figure 8 we used $h = \frac{1}{300} \approx 0.003$ with $\Delta t = 0.0001$.

As can be observed in Figure 8, the unstabilized FEM is unable to numerically simulate the stationary shock and produces a tremendous amount of oscillations. We see the addition of the Vreman stabilization term results in a reduction of the oscillations. We observe a similar phenomena as in the linear case where increasing χ results in a reduction of the oscillations and by $\chi = 0.25$ virtually all oscillations have vanished. Figure 9 plots

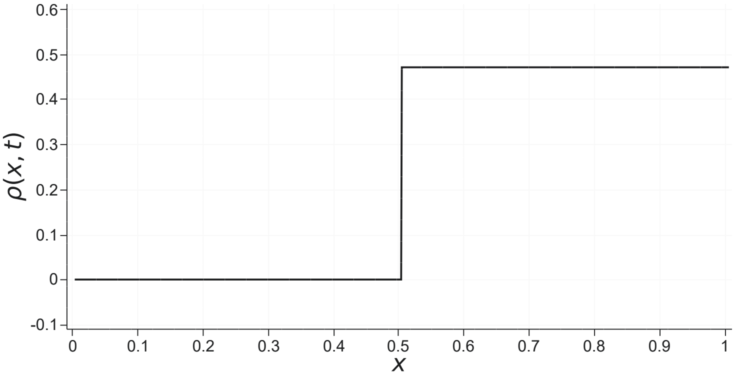

Figure 7: Initial density profile of stationary shock problem.

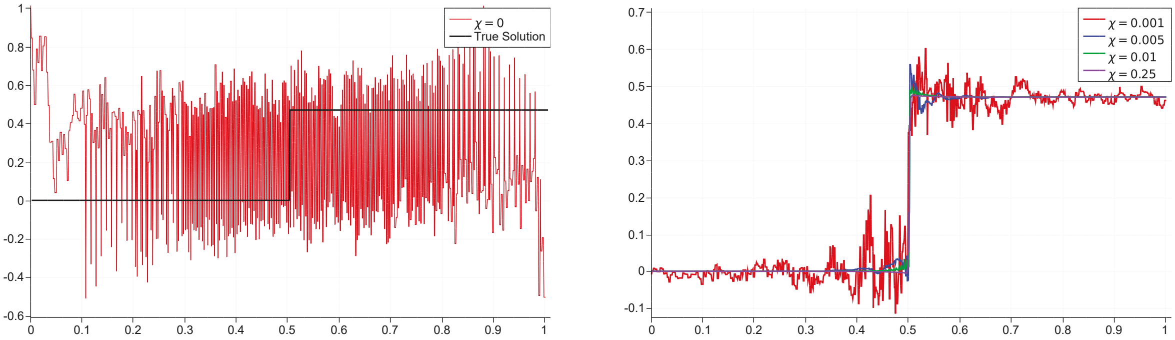

Figure 8: Numerical results of Algorithm 2 with various χ at final time $T = 3$ with $\Delta t = 0.001$, $h \approx 0.003$, $\delta = \sqrt{h}$.

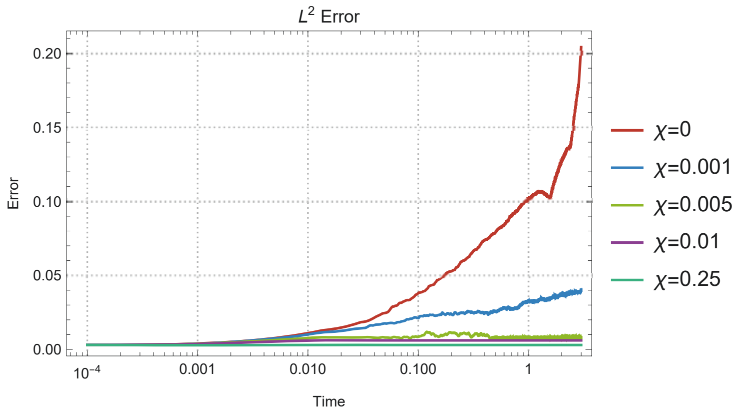

Figure 9: Semi-log plot of L2 errors overtime of Algorithm 2 with various χ and $\Delta t = 0.001$, $h \approx 0.003$, $\delta = \sqrt{h}$.

the $L2$ error of all simulation in Figure 8 over time. This showcases that the addition of χ not only give better qualitative solutions but increases accuracy.

4.5 Discontinuous Initial Density

Here we study the LWR model with the Greenshield's flow velocity relationship as in (1.4). In the context of the motivating biological application, equation (4.5) models the case where the initial density of RNAPs varies along the DNA strand. Initially the density of RNAPs along half of the strand is at its maximum value, and the DNA strand is empty from the midpoint to the right end of the strand. As an example, this could happen when a transcriptional pause has arrested the elongation of those RNAPs traveling on the left half of the strand, while

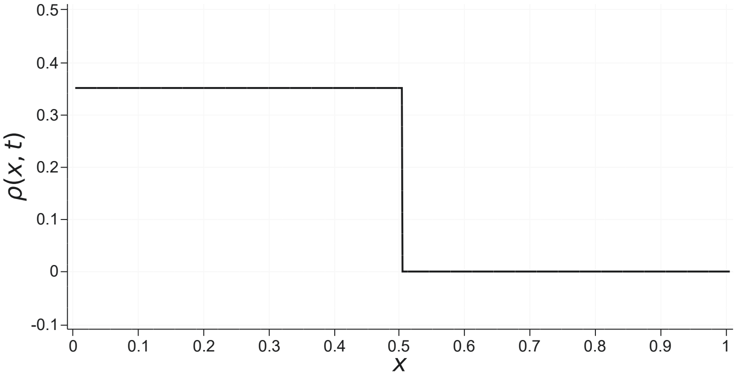

Figure 10: Initial density profile of Discontinuous Initial Density problem.

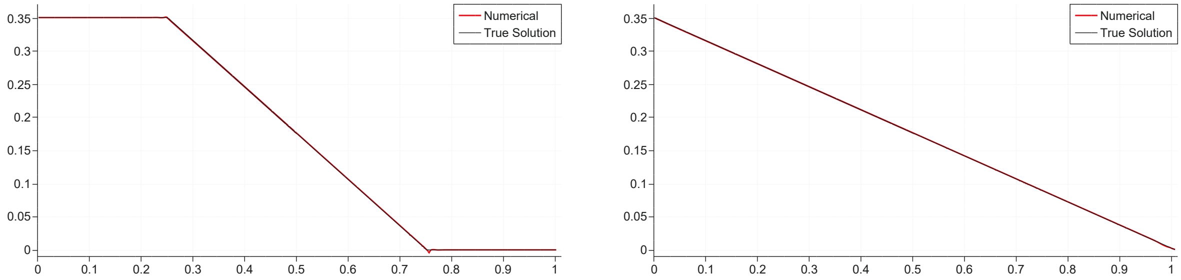

Figure 11: Numerical results of Algorithm 2 at time $t = 0.25$ (left) and $t = 0.5$ (right) with $\Delta t = 0.0001$, $h = 0.002$, $\delta = h$, and $\chi = 1$.

the remainder of the strand has cleared of any other RNAps so that the density on the right half of the strand is set to zero. For $t > 0$, elongation resumes for those RNAPs left on the strand, and a rarefaction wave is formed since $\rho_l > \rho_r = 0$. For this example, we consider the following parameters $\rho_l = 0.35$ and $\rho_r = 0$. We also assign the following parameters the values of $\rho_m = 0.35$, and $v_f = 1$. Based upon the above parameters ρ_l and ρ_r, the initial density profile we get for this problem is shown in Figure 10:

$$\begin{cases} \rho_t + v_f \rho_x - \dfrac{2v_f}{\rho_m}\rho\rho_x = 0, & 0 \le x \le 1,\ 0 < t \le 0.5, \\ \rho(0, t) = 0.35, & t > 0, \\ \rho(x, 0) = \begin{cases} 0.35, & 0 \le x < 0.5, \\ 0, & 0.5 < x \le 1. \end{cases} \end{cases} \tag{4.5}$$

We use $P2$ elements without time filtering for all simulations, and the final time is $T = 0.5$. In Figure 11 we use $h = \frac{1}{500} = 0.002$ with $\Delta t = 0.0001$.

The results in Figure 11 show that the solution behavior of a rarefaction wave is accurately approximated with the numerical scheme in Algorithm 2. This is expected since the solution profile is continuous; however, it should be noted that in such a case, the use of the time filter does not introduce any errors into the approximation scheme in Algorithm 2. This indicates that the time filter can be applied to problems with continuous solutions without concern that the extra step could introduce errors into an accurate approximation to a continuous solution.

5 Conclusion

We consider numerical simulation methods for two models. The first is the linear version of the LWR model in (1.1), and the second model is the nonlinear Greenshield's model primarily known in the study of traffic flow but repurposed here for the biological application of modelling bio-polymerization processes. We investigate the affects of implementing a time filter and stabilization term and present two fully discrete finite element algorithms. Stability is proven in the semi-discrete and fully discrete case. We showcase four numerical simulations for the linear and nonlinear cases and agrees with the literature. The example in Section 4.5 shows that the time filter may be used in a situation where the solution profile is continuous without concern for introducing any extra errors to an otherwise well-behaved solution profile. This is a promising result that warrants future study for cases where a continuous initial condition may lead to a shock developing in time for the case of a nonlinear PDE system.

Funding: The contribution of the authors Dr. Davis and Dr. Pahlevani was supported by the National Science Foundation under Awards DMS-1951510 and DMS-1951563.

References

[1] J. Ahrens, B. Geveci, C. Law, C. Hansen and C. Johnson, Paraview: An end-user tool for large-data visualization, *Visualization Handb.* (2005), 717–731.

[2] N. Bellomo, M. Delitala and V. Coscia, On the mathematical theory of vehicular traffic flow. I. Fluid dynamic and kinetic modelling, *Math. Models Methods Appl. Sci.* **12** (2002), no. 12, 1801–1843.

[3] L. C. Berselli, T. Iliescu and W. J. Layton, *Mathematics of Large Eddy Simulation of Turbulent Flows*, Sci. Comput., Springer, Berlin, 2006.

[4] K. Boatman, L. Davis, F. Pahlevani and T. S. Rajan, Numerical analysis of a time filtered scheme for a linear hyperbolic equation inspired by DNA transcription modeling, *J. Comput. Appl. Math.* **429** (2023), Article ID 115135.

[5] F. Bouchut, *Nonlinear Stability of Finite Volume Methods for Hyperbolic Conservation Laws and Well-Balanced Schemes For Sources*, Front. Math., Birkhäuser, Basel, 2004.

[6] C. A. Brackley, M. C. Romano, M. Thiel, Slow sites in an exclusion process with limited resources, *Phys. Rev. E* **82** (2010), Article ID 051920.

[7] A. Brooks and T. Hughes, Streamline-upwind/Petrov–Galerkin methods for advection dominated flows, *Comput. Methods Appl. Mech. Engrg.* **32** (1980), no. 1–3, 199–259.

[8] G. F. Carey, An analysis of stability And Oscillations In Convection-Diffusion Computations, in: *Finite element methods for Convection Dominated Flows*, ASME, New York (1979), 63–71.

[9] L. Ciandrini, I. Stansfield and M. C. Romano, Role of the particle's stepping cycle in an asymmetric exclusion process: Model of mRNA translation, *Phys. Rev. E* **81** (2010), Article ID 051904.

[10] J. Connors and W. Layton, On the accuracy of the finite element method plus time relaxation, *Math. Comp.* **79** (2010), no. 270, 619–648.

[11] L. Davis, T. Gedeon, J. Gedeon and J. Thorenson, A traffic flow model for bio-polymerization processes, *J. Math. Biol.* **68** (2014), no. 3, 667–700.

[12] L. Davis, T. Gedeon and J. Thorenson, Discontinuous Galerkin calculations for a nonlinear PDE model of DNA transcription with short, transient and frequent pausing, *J. Comput. Math.* **32** (2014), no. 6, 601–629.

[13] L. Davis, F. Pahlevani and T. S. Rajan, An accurate and stable filtered explicit scheme for biopolymerization processes in thepresence of perturbations, *Appl. Comput. Math.* **10** (2021), no. 6, 121–137.

[14] V. DeCaria, S. Gottlieb, Z. J. Grant and W. J. Layton, A general linear method approach to the design and optimization of efficient, accurate, and easily implemented time-stepping methods in CFD, *J. Comput. Phys.* **455** (2022), Article ID 110927.

[15] V. DeCaria, W. Layton and H. Zhao, A time-accurate, adaptive discretization for fluid flow problems, *Int. J. Numer. Anal. Model.* **17** (2020), no. 2, 254–280.

[16] P. P. Dennis, M. Ehrenberg, D. Fange and H. Bremer, Varying rate of RNA chain elongation during rrn transcription in Escherichia coli, *J. Bacteriology* **191** (2009), no. 11, 3740–3746.

[17] A. Dunca and Y. Epshteyn, On the Stolz–Adams deconvolution model for the large-eddy simulation of turbulent flows, *SIAM J. Math. Anal.* **37** (2006), no. 6, 1890–1902.

[18] A. A. Dunca and M. Neda, On the Vreman filter based stabilization for the advection equation, *Appl. Math. Comput.* **269** (2015), 379–388.

[19] T. Dupont, Galerkin methods for first order hyperbolics: an example, *SIAM J. Numer. Anal.* **10** (1973), 890–899.

[20] B. D. Greenshields, A study of traffic capacity, *Highway Res. Board* **14** (1935), 448–477.

[21] V. J. Ervin and E. W. Jenkins, Stabilized approximation to degenerate transport equations via filtering, *Appl. Math. Comput.* **217** (2011), no. 17, 7282–7294.

[22] M. Germano, Differential filters of elliptic type, *Phys. Fluids* **29** (1986), no. 6, 1757–1758.

[23] J.-L. Guermond, Stabilization of Galerkin approximations of transport equations by subgrid modeling, *M2AN Math. Model. Numer. Anal.* **33** (1999), no. 6, 1293–1316.

[24] J.-L. Guermond, Subgrid stabilization of Galerkin approximations of linear monotone operators, *IMA J. Numer. Anal.* **21** (2001), no. 1, 165–197.

[25] A. Guzel and W. Layton, Time filters increase accuracy of the fully implicit method, *BIT* **58** (2018), no. 2, 301–315.

[26] F. Hecht, New development in freefem++, *J. Numer. Math.* **20** (2012), no. 3–4, 251–265.

[27] R. Heinrich and T. A. Rapoport, Mathematical modelling of translation of mrna in eucaryotes: Steady states, time-dependent processes and application to reticulocytes, *J. Theor. Biol.* **86** (1980), 279–313.

[28] V. John and P. Knobloch, On spurious oscillations at layers diminishing (SOLD) methods for convection-diffusion equations. I. A review, *Comput. Methods Appl. Mech. Engrg.* **196** (2007), no. 17–20, 2197–2215.

[29] S. Kang and Y. H. Kwon, A nonlinear Galerkin method for the Burgers equation, *Commun. Korean Math. Soc.* **12** (1997), no. 2, 467–478.

[30] B. L. Keyfitz and M. Shearer, *Nonlinear Evolution Equations that Change Type*, Springer, New York, 1990.

[31] S. Klumpp, Pausing and backtracking in transcription under dense traffic conditions, *J. Stat. Phys.* **142** (2011), 1251–1267.

[32] W. Layton, C. C. Manica, M. Neda and L. G. Rebholz, Numerical analysis and computational testing of a high accuracy Leray-deconvolution model of turbulence, *Numer. Methods Partial Differential Equations* **24** (2008), no. 2, 555–582.

[33] W. J. Layton, C. C. Manica, M. Neda and L. G. Rebholz, Helicity and energy conservation and dissipation in approximate deconvolution LES models of turbulence, *Adv. Appl. Fluid Mech.* **4** (2008), no. 1, 1–46.

[34] W. J. Layton and L. G. Rebholz, *Approximate Deconvolution Models of Turbulence*, Lecture Notes in Math. 2042, Springer, Heidelberg, 2012.

[35] R. J. LeVeque, *Finite Volume Methods for Hyperbolic Problems*, Cambridge Texts Appl. Math., Cambridge University, Cambridge, 2002.

[36] C. T. MacDonald and J. H. Gibbs, Concerning the kinetics of polypeptide synthesis on polyribosomes, *Biopolymers* **7** (1969), 707–725.

[37] C. T. MacDonald, J. H. Gibbs and A. C. Pipkin, Kinetics of biopolymerization on nucleic acid templates, *Biopolymers* **6** (1968), 1–25.

[38] C. C. Manica and S. K. Merdan, Finite element error analysis of a zeroth order approximate deconvolution model based on a mixed formulation, *J. Math. Anal. Appl.* **331** (2007), no. 1, 669–685.

[39] L. Mier-y Terán-Romero, M. Silber and V. Hatzimanikatis, The origins of time-delay in template biopolymerization processes, *PLoS Comput. Biol.* **6** (2010), no. 4, Article ID e1000726.

[40] K. W. Morton and D. F. Mayers, *Numerical Solution of Partial Differential Equations*, 2nd ed., Cambridge University, Cambridge, 2005.

[41] L. B. Shaw, R. K. Z. Zia and K. H. Lee, Totally asymmetric exclusion process with extended objects: A model for protein synthesis, *Phys. Rev. E* **68** (2003), Article ID 021910.

[42] J. Shen and R. Temam, Nonlinear Galerkin method using Chebyshev and Legendre polynomials. I. The one-dimensional case, *SIAM J. Numer. Anal.* **32** (1995), no. 1, 215–234.

[43] F. Spitzer, Interaction of Markov processes, *Adv. Math.* **5** (1970), 246–290.

[44] J. C. Strikwerda, *Finite Difference Schemes and Partial Differential Equations*, 2nd ed., Society for Industrial and Applied Mathematics, Philadelphia, 2004.

[45] V. Thomée and B. Wendroff, Convergence estimates for Galerkin methods for variable coefficient initial value problems, *SIAM J. Numer. Anal.* **11** (1974), 1059–1068.

[46] A. W. Vreman, The filtering analog of the variational multiscale method in large-eddy simulation, *Phys. Fluids* **15** (2003), no. 8, L61–L64.

[47] R. K. P. Zia, J. J. Dong and B. Schmittmann, Modeling translation in protein synthesis with TASEP: A tutorial and recent developments, *J. Stat. Phys.* **144** (2011), no. 2, 405–428.